One-Dimensional Gold Nanostructures through Directed Anisotropic Overgrowth from Gold Decahedrons

Daeha Seo,[†] Jun Hui Park,[†] Jongwook Jung,[†] Seung Min Park,[‡] Seol Ryu,[‡] Juhyoun Kwak,[†] and Hyunjoon Song*,[†]

Department of Chemistry and School of Molecular Science (BK21), Korea Advanced Institute of Science and Technology, Daejeon 305-701, Korea, and Department of Chemistry, Kyung Hee University, Seoul 130-701, Korea

Received: October 22, 2008; Revised Manuscript Received: January 4, 2009

One-dimensional gold nanorods were synthesized from gold decahedrons in the presence of silver ions by a systematic overgrowth approach. Both the diameters and lengths of the nanorods were independently varied by using distinct-sized decahedrons and gold precursor concentrations. The key factors of anisotropic growth are three-dimensional decahedral seed structures and energetic differentiation of the distinct facets. A series of copper and silver underpotential deposition (UPD) experiments confirmed that the silver components were mainly located on the Au(100) facets, which constitute the side walls of the nanorods. The growth mechanism of the gold nanorods could be clarified by an arbitrary elongation of the decahedral seeds and selective restriction of the {100} growth by silver UPD. Low temperature growth without silver generated very long nanowires by preferential adsorption of poly(vinyl pyrrolidone) on the {100} surface.

Introduction

Recent development of shape control in gold nanostructures enables us to make various polyhedrons such as cubes, cuboctahedrons, octahedrons, decahedrons, icosahedrons, and truncated octahedrons and adjust their physical properties precisely.[1−3] Synthesis of anisotropic structures such as gold nanorods and wires has also been widely studied since El-Sayed's[4] and Murphy's[5] pioneering works and has attracted much attention due to the fine-tuning of light scattering from visible to near-infrared regions by changing their aspect ratios (length/diameter). These unique optical properties of the one-dimensional gold nanostructures have been exploited in sensing, imaging, and photothermal therapy.[6,7]

Murphy's nanorod synthesis is based on a seed-mediated growth in aqueous solution in the presence of cetyltrimethylammonium bromide (CTAB). This process is under mild conditions at room temperature and is readily scalable up to grams.[5,8] The fundamental understanding of such an anisotropic growth is significant because the face-centered cubic metals like gold have no crystallographic driving force for directionality. The formation mechanism of gold nanorods is, however, rather ambiguous because of the various reagents used under the complex reaction conditions. The key factors of the reaction are not only the concentrations of gold precursor and reducing agent but also those of cationic surfactants, counteranions, and metal additives such as silver ions. It is postulated that crystalline seed structures and preferential surfactant binding to the certain facets of the seeds are critical to the nanorod growth, but there are other proposed mechanisms reported as well.[9] The other questionnaire is the role of silver ions during the reaction, which increased the total yield of nanorods up to ∼100% but discriminated their aspect ratio to less than 6.[10] The light-induced gold rod formation also requires silver ions necessarily.[11]

SCHEME 1: Anisotropic Growth of Gold Nanorods from Gold Decahedrons

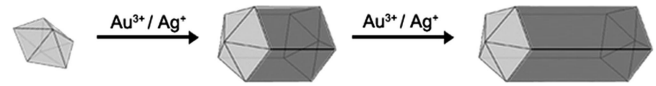

Recently, the gold nanorod growth without adding silver ions was also reported.[12]

In the present study, we have synthesized gold nanorods by a systematic overgrowth approach from gold decahedrons in the presence of silver ions. Both diameters and lengths of the nanorods were independently varied by using distinct sized decahedrons and gold precursor concentrations (Scheme 1). The anisotropic growth of the nanorods originates from the combination of three-dimensional decahedral structures and energetic differentiation of the walls and tips in gold nanorods by preferential underpotential deposition (UPD) of silver, which could be confirmed by electrochemical analysis. Gold nanowires with the aspect ratio of ∼200 were also synthesized from the gold decahedrons without silver ions, resulting from the preferential adsorption of poly(vinyl pyrrolidone) (PVP) on the walls of nanowires.

Experimental Methods

Synthesis of Gold Nanorods (Sample A). High-purity $HAuCl_4$ and the decahedrons with average edge sizes of 40 and 64 nm were prepared according to the literature.[3b] For the thin nanorods, a $AgNO_3$ (99+%, Aldrich) solution (0.15 mL) in 1,5-pentanediol (PD, 96%, Aldrich) was added to the boiling PD solution containing small decahedrons (5.0 mL, 2.1 mM with respect to the gold precursor concentration). Immediately, PVP (total 3.0 mL, M_w = 55000, Aldrich) and $HAuCl_4$ (total 3.0 mL) PD solutions were added periodically every 30 s over 7.5 min. The resulting mixture was heated at reflux for 7.5 min. The products were repeatedly washed with ethanol (99.9%, J. T. Baker) in a precipitation/dispersion cycle. The concentrations

* To whom correspondence should be addressed. E-mail: hsong@kaist.ac.kr.
[†] Korea Advanced Institute of Science and Technology.
[‡] Kyung Hee University.

10.1021/jp8093337 CCC: $40.75
Published on Web 02/05/2009

of $AgNO_3$, PVP, and $HAuCl_4$ solutions in PD used for the reactions were 1.2, 36, and 8.5 mM for the short rods, 2.0, 61, and 17 mM for the medium rods, and 2.9, 86, and 25 mM for the long rods, respectively. For the thick nanorods, all procedures were identical to those of the thin rods except the use of large decahedrons with an edge size of 64 nm.

Removing Surface Silver Species (Sample B). The gold nanorods were deposited either on the silicon wafer (P-100, 1 cm × 1 cm) for X-ray photoelectron spectroscopy (XPS) measurements or on the indium tin oxide (ITO) electrodes (0.246 cm^2) for electrochemical analyses by drop casting. The resulting substrates were immersed in $HAuCl_4$ aqueous solution (3.0 mL, 5.0 mM) at room temperature for 2 h and thoroughly washed with ammonia solution (28.0∼30.0%, Junsei).

Metal UPD Experiments. A glass coated with ITO (50 Ω, JMI Korea) was used as an electrode in order to prevent unwanted UPD in the given system. The geometrical electrode area was 0.246 cm^2. The stock solutions were prepared with ultrapure water (>18 MΩ, Millipore Milli-Q purification system). Cyclic voltammetry was performed with a Pt counter electrode with either Ag or Cu wires as a reference electrode connected to an electrochemical cell via a capillary salt bridge. The solutions were purged with argon before use, and the argon atmosphere was maintained during all measurements. Potential control and sweeps were conducted with a CHI900B (CH Instruments, Austin, TX) electrochemical analyzer. For the preparation of gold nanorod films on the ITO electrode, a colloidal dispersion of gold nanorods (0.030 mL, 17 mM with respect to the gold precursor concentration) was casted on the ITO surface. The samples were exposed to oxygen plasma for 5 min. For Cu UPD experiments, the copper deposition solution was 0.1 M H_2SO_4 (95%, Junsei) solution containing 1.0 mM $CuSO_4$ (99.999%, Aldrich). The applied potential was cyclically swept from 0.65 to 0.03 V vs the Cu wire reference electrode. For Ag UPD experiments, the silver deposition solution was 0.1 M H_2SO_4 solution containing 1.0 mM Ag_2SO_4 (99.999%, Aldrich). The applied potential was cyclically swept from 0.55 to 0 V versus the Ag wire reference electrode. The scan rates for the electrochemical anayses were set to 5 mV s^{-1}.

Discrete Dipole Approximation (DDA) Calculation for Nanorods. The DDA method has been described in detail elsewhere.[13,14] DDA calculation approximates a metal particle as a collection of induced dipoles in a small unit interacting with each other and an incident light. In this work, the decahedral gold nanorods of various aspect ratios are modeled with point dipoles in the cubic lattice of about 2 nm grid spacing. The thin nanorods of aspect 1.8, 2.0, and 2.4 are constructed with 33244, 52923, and 116240 point dipoles, respectively. Also, the thick ones with 2.0, 2.3, and 2.6 are with 33244, 52923, and 116240, respectively. The DDSCAT code developed by Draine and Flatau[13] was used to calculate the extinction cross section for each nanorod structure for a given wavelength of an incident light. The extinction spectrum was averaged rotationally over 48 orientations of the nanoparticle relative to the direction of incident light. To introduce effects of size distributions in spectra, we modulated the aspect ratio of each structure by ±0.5 while keeping the constant particle volume and assumed that each modulated structure makes 20% spectral contribution to the total spectrum. The 2:6:2 contributions of such three (elongated, original, and compressed) structures were found to be representative of nanorod samples, and the corresponding theoretical spectra resulted in peak broadenings comparable to those found in the corresponding experimental ones. However, the spectra of decahedral structures prior to overgrowth were well matched with the theoretical spectra of single model geometries (5580 and 21723 point dipoles for thin and thick ones, respectively). The dielectric medium (solvent) was chosen to be water and the wavelength of incident light was varied with an interval of 10 nm. The dielectric function of gold has been taken from the literature.[15]

Synthesis of Gold Nanowires. The decahedral seeds with an average diameter of 37 ± 5 nm (13 μmol with respect to the gold precursor concentration) were dispersed in tetraethylene glycol (15 mL, TEG, 99%, Aldrich) in the presence of PVP (1.0 g, 360 equiv) at 100 °C. A $HAuCl_4$ solution (1.0 mL, 25 mM) in TEG was added, and the resulting mixture was heated at 100 °C for 24 h. The product was collected by centrifugation and was repeatedly washed with ethanol in a precipitation/dispersion cycle.

Results and Discussion

Synthesis of Gold Nanorods from Small and Large Gold Decahedrons. The gold nanorod synthesis was based on the overgrowth of gold decahedral seeds through a modified polyol process. Briefly, 1/200 equiv of $AgNO_3$ with respect to the gold precursor concentration was added to the colloidal dispersion of gold decahedrons in boiling PD. Appropriate amounts of PVP and $HAuCl_4$ PD solutions were added periodically every 30 s over 7.5 min to the reaction mixture, followed by refluxing for 7.5 min. The product was repeatedly washed with ethanol in a precipitation/dispersion cycle. When small decahedrons with an average edge length of 40 ± 5 nm (Figure 1a) were used as a seed surface, thin nanorods were obtained as a major product (Figure 1). The more the gold precursor amount was added to the reaction mixture, the longer the resulting nanorods became. As shown in parts b−d of Figure 1, the length and diameter (aspect ratio) of each nanorod varied from 112 ± 15, 61 ± 7 nm (1.8 ± 0.2) to 145 ± 22, 68 ± 9 nm (2.1 ± 0.3), and 199 ± 25, 78 ± 10 nm (2.4 ± 0.3), respectively. The tilted scanning electron microscopy (SEM) image of the longest nanorods by 45° (Figure 2) clearly shows the three-dimensional rod structure with a pentagonal cross-section and half-decahedral tips. Transmission electron microscopy (TEM) image shows a projection of the nanorod structure, and selected area electron diffraction (SAED) pattern includes two sets of spots along the zone axes corresponding to [001] and [1−1−2] (Figure 3), which exactly match the results from multiply twinned nanorods of Au, Ag, and Cu.[16] The growth direction of the rods is [110].

Larger decahedrons produced thicker nanorods. The decahedrons with an edge length of 64 ± 6 nm (Figure 1e) yielded the nanorods with average lengths and diameters (aspect ratios) of 160 ± 16 and 89 ± 10 nm (1.8 ± 0.3) in Figure 1f, 200 ± 20 and 97 ± 10 nm (2.1 ± 0.3) in Figure 1g, and 282 ± 23, 112 ± 11 nm (2.5 ± 0.3) in Figure 1h, respectively. As the gold precursor concentration increased, both length and diameter of the nanorods increased at the same time, but the relative ratio of the increments (length/diameter) is larger than 10, indicating the preferential anisotropic growth of nanorods along the longitudinal direction.

Critical Factors for Anisotropic Gold Nanorod Growth. There are two critical factors for the origin of anisotropic growth in gold nanorod formation. First, the original seed structure serves as an active surface to enhance epitaxial deposition of the gold atoms and guides an initial growth direction. Murphy's nanorod synthesis uses tiny single crystalline seeds,[17] but the final product contains multiple twin planes. In the formation of silver nanowires, 5-fold twinned particles were demonstrated as initial seeds.[18] To understand the importance of crystal-

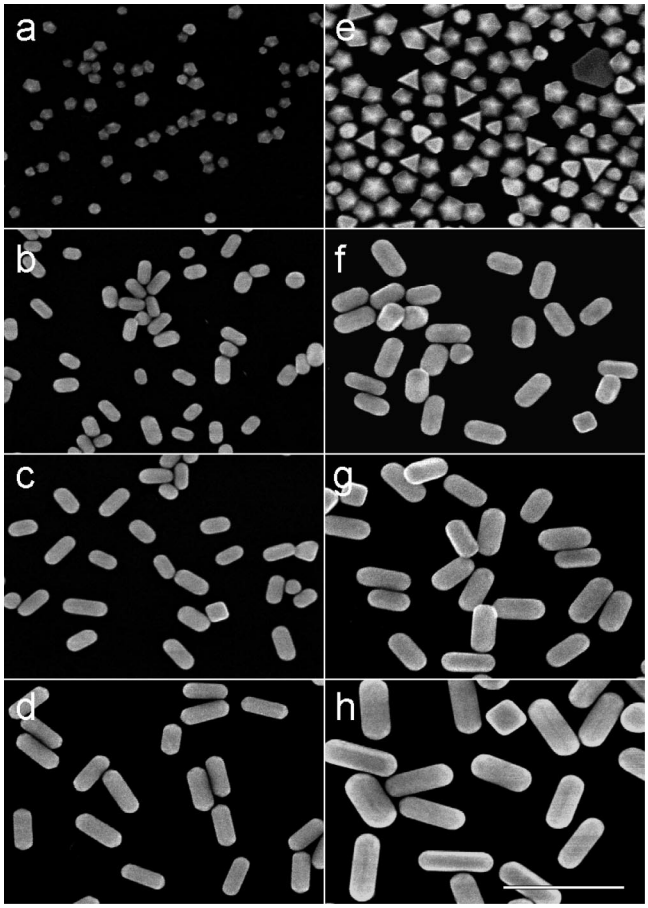

Figure 1. SEM images of (a) small gold decahedrons with an average edge length of 40 ± 5 nm, (b−d) thin gold nanorods grown from small decahedrons, (e) large decahedrons with an average edge length of 64 ± 6 nm, and (f−h) thick nanorods grown from large decahedrons. The bar represents 500 nm.

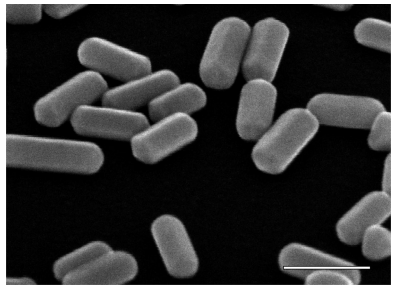

Figure 2. Tilted SEM image of the long nanorods grown from the small gold decahedrons with an edge size of 40 nm by 45°. The bar represents 200 nm.

lographic twinning, gold icosahedrons with an edge size similar to that of the gold decahedrons were used under the growth condition, because the icosahedron has a 5-fold symmetry with a multiply twinned crystal structure, identical to that of the decahedron.[3b] However, the grown particles were still rounded without any elongation, revealing that the three-dimensional decahedral structure is the main concern of anisotropy. The ideal pentagonal rods contain {111} facets at the half-decahedral tip regions and {100} surfaces on the walls. The interfacial angles between triangular faces at the tips and adjacent walls are 53.6° in the three-dimensional rod structure, which is close to the crystallographic dihedral angle of 54.7° between {111} and {100} faces. This gives a minimum structural stress to promote anisotropic growth along the [110] direction on the decahedral

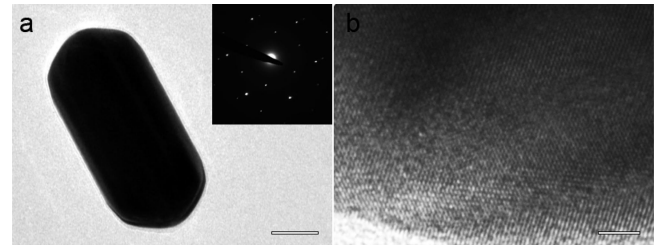

Figure 3. (a) TEM image and SAED pattern (inset) and (b) HRTEM image of a gold nanorod. The bars represent (a) 40 nm and (b) 2 nm.

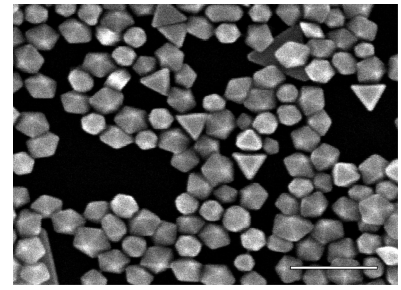

Figure 4. SEM image of the product grown from the decahedrons with an average edge size of 40 ± 5 nm without $AgNO_3$ addition. The average edge size of the product is estimated to be 54 ± 5 nm. The bar represents 200 nm.

shapes, and thereby the crystal grows along the longitudinal axis continuously (vide infra).

Second, an energetic differentiation of distinct facets between {111} and {100} must be provided under the reaction conditions. In Murphy's nanorod synthesis, CTAB is proposed to be preferentially bound on the {100} facets of the walls, where the size of the surfactant headgroups is more comparable than the {111} faces.[5a] Silver nanowire formation also relies on the preferential interaction of PVP onto {100} faces to the {111} surface.[18] In our experiments, the overgrowth of decahedral seeds without $AgNO_3$ yielded large decahedrons with an average edge size of 54 ± 5 nm, as shown in Figure 4. This indicates that Ag ions are crucial for the directional growth of decahedrons. In the overgrowth of octahedrons, it is suggested that silver is preferentially deposited onto the {100} surface under the condition of underpotential deposition (UPD) and lowers the growth rate of {100} and/or enhances that of {111}, yielding uniform cubes eventually.[3] Guyot-Sionnest et al. suggested that Ag UPD could also account for the gold rod formation in the presence of silver ions.[19] If the Ag UPD is still the major mechanism of our nanorod synthesis, most of the silver residues should be detected on the {100} faces (or on the walls) but not on the {111} faces (or on the tips). To confirm the selective deposition of silver, we examined a series of surface and electrochemical experiments. X-ray diffraction (XRD) spectrum of the gold nanorods exhibits intense (111) and (200) peaks at 38.3 and 44.5°, respectively, whereas the original decahedrons have only a strong (111) peak due to the regular particle orientation against the substrate (Figure 5a). It definitely reveals the generation of {100} facets during the rod formation. XPS results show no peak in the Ag 3d region for the decahedrons but exhibit two strong Ag $3d_{3/2}$ and $3d_{5/2}$ bands for the nanorods (Figure 5b, top, solid line). The silver composition with respect to that of gold was quantitatively estimated to be 11.6 at % from the relative intensity of silver 3d and gold 4f bands with corresponding atomic conversion factors, although the original usage of $AgNO_3$ is 0.5 at %. It indicates that most silver atoms are located on the gold surface within the depth of ~2 nm. These

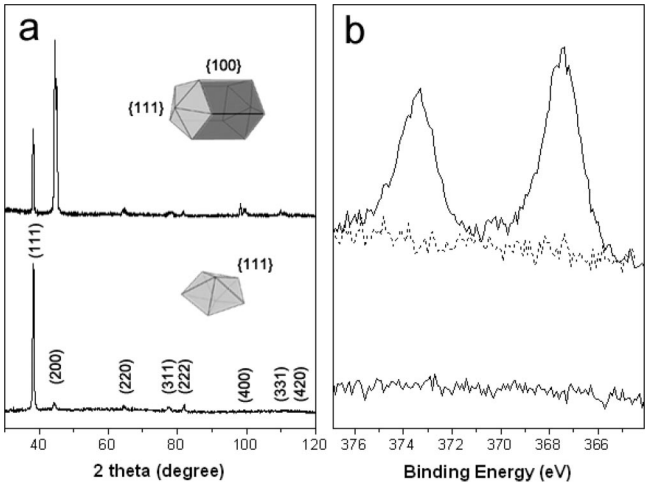

Figure 5. (a) XRD spectra of gold decahedrons (bottom) and rods (top). (b) XPS spectra of gold decahedrons (bottom), rods (sample A, top, solid line), and rods after removing Ag components (sample B, top, dotted line) in the Ag 3d region.

silver atoms were successfully removed by the treatment with weak $HAuCl_4$ and ammonia solutions in sequence. Surface Ag atoms could be replaced by gold atoms through the Galvanic exchange reaction, and the resulting silver ions and silver chlorides were washed with ammonia solution. The dotted line of Figure 5b shows no detectable silver components in the XPS spectrum after the washing process.

UPD Experiments. Electrochemical deposition experiments were performed for the gold nanorods before (sample A) and after Ag removal (sample B) on ITO electrodes. Figure 6a shows cyclic voltammograms (CVs) of the electrodes in 0.1 M H_2SO_4 containing 1.0 mM $CuSO_4$ with the scan rate of 5 mV s^{-1}. In this condition, Cu UPD takes place on the Au(111) single crystalline surface at 0.065 and 0.205 V and on the Au(100) surface at 0.240 V vs Cu/Cu^{2+}, respectively.[20] It is noted that Cu UPD does not occur on Ag(*hkl*).[21] The CV of sample A (solid line) exhibits two sharp peaks assignable to the Cu UPD on Au(111) but does not show distinguishable signals in the range of 0.22−0.25 V. In contrast, the CV of sample B (dotted line) shows a clear peak assignable to Au(100) at 0.240 V as well as two Au(111) peaks. It represents that the Au(111) surface of sample A is relatively clean, but the Au(100) surface is contaminated by the silver components, blocking Cu UPD effectively. For a quantitative analysis, total charges for Cu desorption were calculated by the integration of the signals in the different potential ranges. The charge increment between samples A and B (7.2 and 8.9 C) is 23% in the range of 0.0−0.1 V (D2) including the Au(111) peak at 0.065 V. On the other hand, the charge increases by 73% (54 and 94 C) at the range of 0.1−0.4 V (D1), where both Au(111) and (100) peaks are included, as summarized in Figure 6c. This result implies that most silver atoms covered the Au(100) faces of sample A, and thereby removing the silver species (sample B) increases the exposed Au(100) surface significantly.

Because of the overlapping of Au(111) and Au(100) peaks in the CV of Cu UPD, Ag UPD experiments were carried out for an accurate analysis. The Ag UPD on Au(100) shows three distinct adsorption peaks, of which two peaks at 0.03 and 0.52 V are overlapped with Au(111) peaks (A1 and A3), but one peak at 0.280 V vs Ag/Ag^+ is completely isolated from the other peaks, respectively.[22] Figure 6b presents CVs of samples A (solid line) and B (dotted line) in the 0.1 M H_2SO_4 solution containing 1.0 mM Ag_2SO_4. Since Ag UPD does not occur on

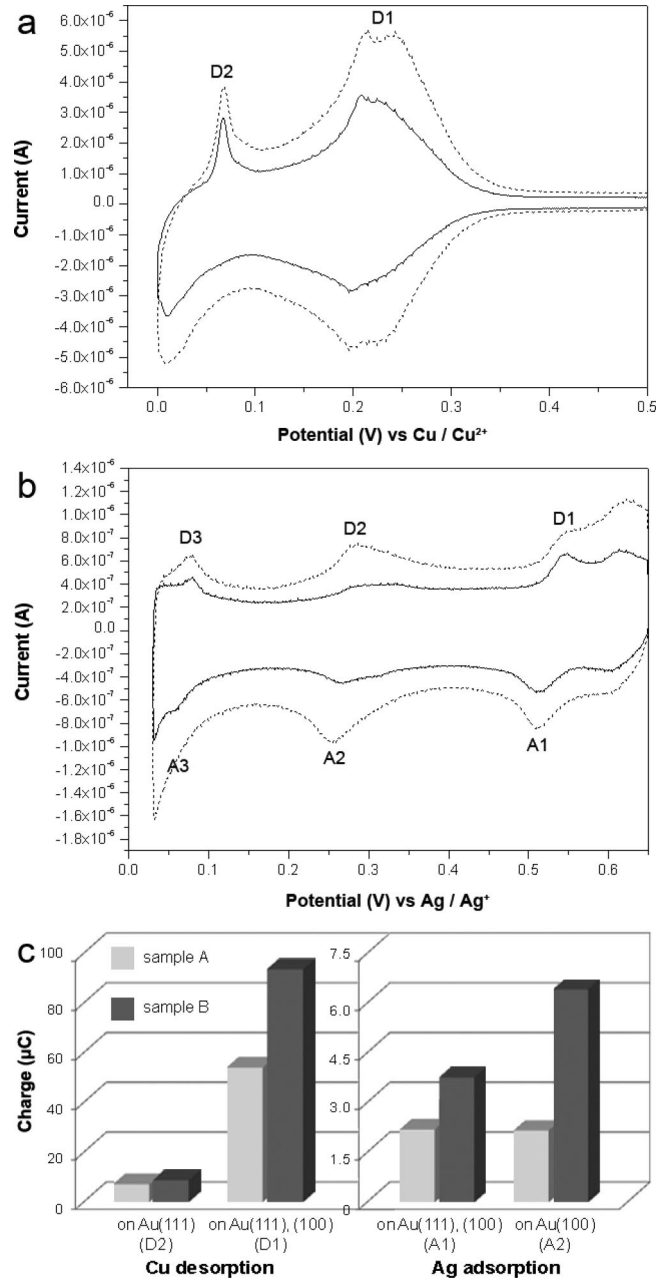

Figure 6. CVs of (a) Cu and (b) Ag UPDs on sample A (solid lines) and sample B (dotted lines) at the scan rate of 5 mV s^{-1}. Dn and An indicate the ranges where the desorption and adsorption of metal species take place, respectively. (c) The change of desorption and adsorption charges of samples A and B.

the silver surface, the CV of sample A exhibits a very broad signal at 0.2−0.4 V (A2) assigned to the adsorption on Au(100). But in sample B, the Au(100) peak at A2 is larger than the intensity of the other peaks at A1 and A3. The absolute value of the adsorption charge of sample B increases by 72% compared to that of sample A for the Au(111) peaks (−2.2 and −3.8 C, A1), but the charge difference of samples A and B is 200% (−2.2 and −6.4 C) at A2 as presented in Figure 6c. The silver adsorption on the Au(100) surface is not completely zero because silver residues were inhomogeneously deposited on the Au(100) faces during the rod formation. The theoretical simulation shows that Ag UPD commonly grows silver islands rather than closed-packed monolayers on the gold surface.[23] From the Cu and Ag deposition results for samples A and B, it is concluded that most silver species on the gold nanorods are

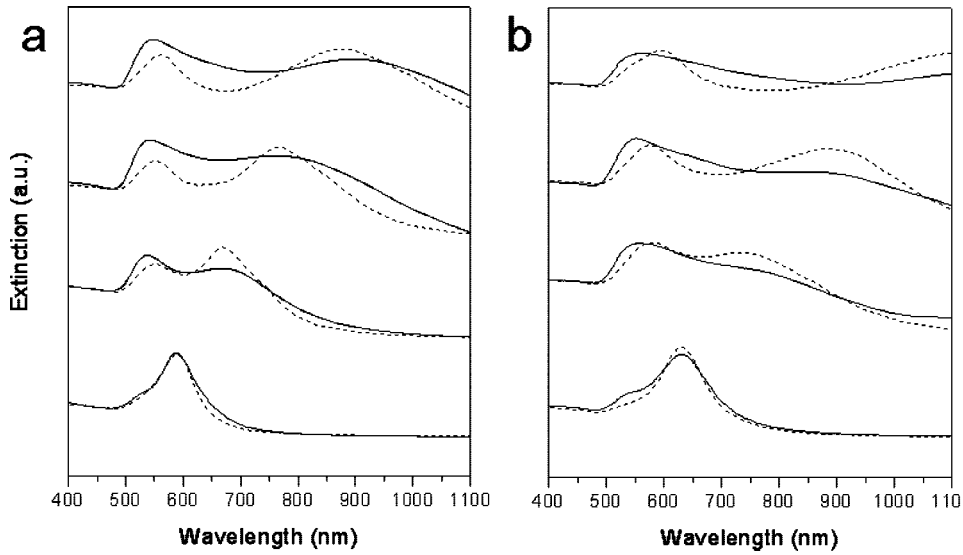

Figure 7. UV−vis spectra (solid line) and theoretical calculations (dotted line) of (a) small decahedrons and thin gold nanorods with the average aspect ratios of 1.8, 2.1, and 2.4 from bottom to top and (b) large decahedrons and thick gold nanorods with the average aspect ratios of 1.8, 2.1, and 2.5 from bottom to top, respectively.

placed on the {100} faces and block the surface against further deposition. The growth of {100} faces by the gold atom deposition may also be hindered by the existence of Ag residues, and thereby the growth takes place on the {111} facets of the tips along the longitudinal direction. The similar selective deposition of Pt was observed on the gold nanorods by the assistance of silver ions.[24]

Formation Mechanism of Gold Nanorods. By consideration of the two critical factors, three-dimensional structure of decahedral seeds and preferential Ag UPD on Au(100), the mechanism of the gold nanorod formation from decahedrons is postulated. The gold atoms reduced from the reaction mixture are deposited on the decahedral surface. If any of Au(100) starts to form by random deposition of the gold atoms, Ag species selectively bind to Au(100) and hinders further growth along that direction. The more the gold atoms are deposited on the seed surface, the more the {100} facets are generated and finally form elongated decahedrons as a stable structure. Because of the unique three-dimensional architecture of the decahedrons, structural elongation extends the {100} faces on the walls, and silver UPD continuously restrict the {100} growth rate. Consequently, the {111} facets of the tips preferentially grow along the [110] direction to obtain longer nanorods with a high aspect ratio.

Optical Spectra and Theoretical Simulations. The optical property of the gold nanorods is very sensitive to their aspect ratio. The UV−vis extinction of each nanorod was measured and simulated by DDA.[13] Figure 7 shows the measured and theoretical spectra of the nanorods with various aspect ratios. The two extinction peaks normally appear in the spectrum, where the peaks at longer and shorter wavelength are assigned to longitudinal and transversal plasmon excitations, respectively. As the aspect ratio of the thin nanorods increases from 1.8 to 2.4 (Figure 7a), the longitudinal plasmon mode shifts linearly from 670 nm to the lower energy up to near IR (890 nm), while the transverse mode stays at a constant wavelength of ~540 nm. The plasmon modes of the thick nanorods also exhibit similar trends to those of the thin rods (Figure 7b). The experimental data have broader peaks than the theoretical results, because of the fact that the real nanorods have relatively wide length and diameter distributions, but the maximum of each peak is nearly identical to the calculation value.

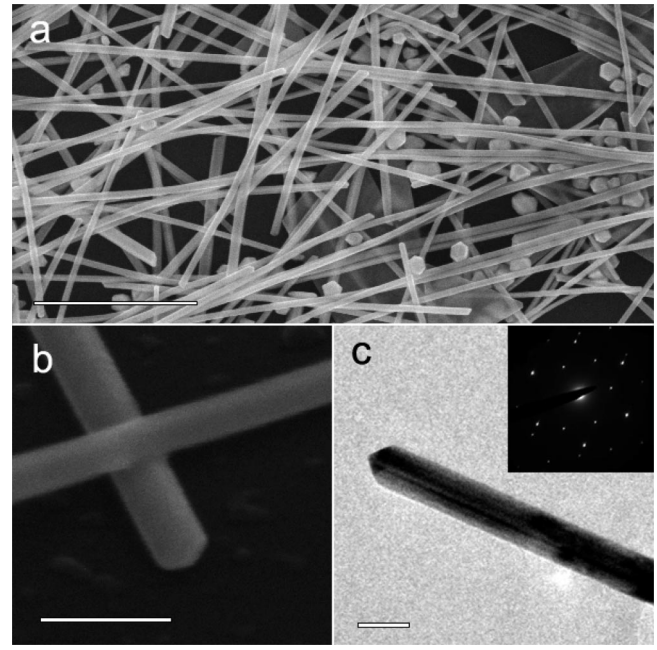

Figure 8. (a) SEM image of gold nanowires. (b) Tilted SEM image of gold nanowires by 45°. (c) TEM image and SAED pattern (inset) of a gold nanowire. The bar represents (a) 2 μm, (b) 100 nm, and (c) 60 nm.

Synthesis of Gold Nanowires. The gold nanowires with a high aspect ratio of ~200 were synthesized through a similar polyol process without $AgNO_3$ addition. $HAuCl_4$ was added to the reaction mixture containing small gold decahedrons with an edge length of 37 ± 5 nm in TEG in the presence of excess PVP. The mixture was heated at 100 °C for 24 h to yield gold nanowires in a high yield. Large triangular plates and self-seeded particles were byproducts with a total yield of less than 30%. Figure 8a shows that an average diameter of the wires is estimated to be 50 ± 6 nm with the length of ~10 μm. The tilted SEM image by 45° in Figure 8b roughly represents a sharp tip of a nanowire, implying that the half-decahedral structure is still maintained at the tip region. The TEM image and SAED pattern in Figure 8c exhibits cyclic pentatetrahedral twins of the nanowire, exactly matching with those of the gold nanorods

synthesized by a seed-mediated growth with CTAB.[5] In the formation mechanism, the decahedral seeds are still a critical requirement for the anisotropic growth, but the reaction condition is quite different from the nanorod synthesis. The preferential adsorption of PVP onto {100} faces plays an important role for the differentiation of distinct facets, which is already reported in the silver nanowire formation by Xia et al.[18] Murphy et al. synthesized gold nanorods with a high aspect ratio in the absence of silver ions,[17] presumably following the mechanism similar to that of silver nanowires. A few recent papers also reported the similar seed-mediated gold nanowire growth with high aspect ratios.[26] It is anticipated that the decahedrons were continuously grown under this reaction condition to yield gold nanowires until all gold precursors were consumed, whereas the addition of $AgNO_3$ at high temperature lowers the total growth rate of gold nanorods and restrict their aspect ratio below a certain threshold.

Conclusions

We have synthesized one-dimensional gold nanorods and nanowires by a systematic overgrowth from gold decahedrons. The key factors of anisotropy are (i) three-dimensional decahedral seed structures and (ii) energetic differentiation of the distinct facets. The addition of $AgNO_3$ induces a selective silver UPD onto the {100} facets and forms gold nanorods with small aspect ratios of 1.8−2.6, and the low temperature growth without silver generates very long gold nanowires by a preferential adsorption of PVP on the {100} surface. It is anticipated that this approach can provide a rational design of anisotropic growth for other metal and metal oxide systems. It can be also applied for the synthesis of multisegmented superlattice structures by heterometal deposition.[24,25]

Acknowledgment. This work was supported by the Nano R&D Program (2007-02668) and a grant from the Korea Science and Engineering Foundation (KOSEF), funded by the Korean Government (MEST) (No. R11-2007-050-04002-0). J.K. acknowledges the support by the Nano/Bio Science & Technology Program (2005-01333) of the Ministry of Education, Science and Technology.

References and Notes

(1) (a) Tao, A. R.; Habas, S.; Yang, P. *Small* **2008**, *4*, 310. (b) Kim, F.; Connor, S.; Song, H.; Kuykendall, T.; Yang, P. *Angew. Chem., Int. Ed.* **2004**, *43*, 3673.

(2) (a) Sau, T. K.; Murphy, C. J. *J. Am. Chem. Soc.* **2004**, *126*, 8648. (b) Sánchez-Iglesias, A.; Pastoriza-Santos, I.; Pérez-Juste, J.; Rodríguez-González, B.; García de Abajo, F. J.; Liz-Marzán, L. M. *Adv. Mater.* **2006**, *18*, 2529. (c) Chen, Y.; Gu, X.; Nie, C.-G.; Jiang, Z.-Y.; Xie, Z.-X.; Lin, C.-J. *Chem. Commun.* **2005**, 4181.

(3) (a) Seo, D.; Yoo, C. I.; Park, J. C.; Park, S. M.; Ryu, S.; Song, H. *Angew. Chem., Int. Ed.* **2008**, *47*, 763. (b) Seo, D.; Yoo, C.; Chung, I. S.; Park, S. M.; Ryu, S.; Song, H. *J. Phys. Chem. C* **2008**, *112*, 2469. (c) Seo, D.; Park, J. C.; Song, H. *J. Am. Chem. Soc.* **2006**, *128*, 14863.

(4) (a) El-Sayed, M. A. *Acc. Chem. Res.* **2001**, *34*, 257. (b) Eustis, S.; El-Sayed, M. A. *Chem. Soc. Rev.* **2006**, *35*, 209.

(5) (a) Murphy, C. J.; Sau, T. K.; Gole, A. M.; Orendorff, C. J.; Gao, J.; Gou, L.; Hunyadi, S. E.; Li, T. *J. Phys. Chem. B* **2005**, *109*, 13857, and references therein. (b) Murphy, C. J.; Sau, T. K.; Gole, A.; Orendorff, C. J. *MRS Bull.* **2005**, *30*, 349.

(6) (a) Lee, K.-S.; El-Sayed, M. A. *J. Phys. Chem. B* **2006**, *110*, 19220. (b) Pérez-Juste, J.; Pastoriza-Santos, I.; Liz-Marzán, L. M.; Mulvaney, P. *Coord. Chem. Rev.* **2005**, *249*, 1870. (c) Murphy, C. J.; Gole, A. M.; Hunyadi, S. E.; Stone, J. W.; Sisco, P. N.; Alkilany, A.; Kinard, B. E.; Hankins, P. *Chem. Commun.* **2008**, 544.

(7) (a) Huang, X.; El-Sayed, I. H.; Qian, W.; El-Sayed, M. A. *J. Am. Chem. Soc.* **2006**, *128*, 2115. (b) Ding, H.; Yong, K.-T.; Roy, I.; Pudavar, H. E.; Law, W. C.; Bergey, E. J.; Prasad, P. N. *J. Phys. Chem. C* **2007**, *111*, 12552.

(8) Jana, N. R. *Small* **2005**, *1*, 875.

(9) (a) Pérez-Juste, J.; Liz-Marzán, L. M.; Carnie, S.; Chan, D. Y. C.; Mulvaney, P. *Adv. Funct. Mater.* **2004**, *14*, 571. (b) Diao, J.; Gall, K.; Dunn, M. L. *Nat. Mater.* **2003**, *2*, 656.

(10) Sau, T. K.; Murphy, C. J. *Langmuir* **2004**, *20*, 6416.

(11) Kim, F.; Song, J. H.; Yang, P. *J. Am. Chem. Soc.* **2002**, *124*, 14316.

(12) Orendorff, C. J.; Murphy, C. J. *J. Phys. Chem. B* **2006**, *110*, 3990.

(13) (a) Yang, W.-H.; Schatz, G. C.; Van Duyne, R. P. *J. Chem. Phys.* **1995**, *103*, 869. (b) Draine, B. T.; Flatau, P. J. *Program DDSCAT*, Scripps Institute of Oceanography, University of California, San Diego, CA.

(14) (a) Draine, B. T.; Flatau, P. J. *J. Opt. Soc. Am. A* **1994**, *11*, 1491. (b) Kelly, K. L.; Coronado, E.; Zhao, L. L.; Schatz, G. C. *J. Phys. Chem. B* **2003**, *107*, 668.

(15) Johnson, P. B.; Christy, R. W. *Phys. Rev. B* **1972**, *6*, 4370.

(16) (a) Johnson, C. J.; Dujardin, E.; Davis, S. A.; Murphy, C. J.; Mann, S. *J. Mater. Chem.* **2002**, *12*, 1765. (b) Lisiecki, I.; Filankembo, A.; Sack-Kongehl, H.; Weiss, K.; Pileni, M.-P.; Urban, J. *Phys. Rev. B* **2000**, *61*, 4968. (c) Sun, Y.; Xia, Y. *Adv. Mater.* **2004**, *16*, 264.

(17) Gole, A.; Murphy, C. J. *Chem. Mater.* **2004**, *16*, 3633.

(18) (a) Chen, J.; Wiley, B. J.; Xia, Y. *Langmuir* **2007**, *23*, 4120. (b) Sun, Y.; Mayers, B.; Herricks, T.; Xia, Y. *NanoLett.* **2003**, *3*, 955.

(19) Liu, M.; Guyot-Sionnest, P. *J. Phys. Chem. B* **2005**, *109*, 22192.

(20) Kuzume, A.; Herrero, E.; Feliu, J. M.; Nichols, R. J.; Schiffrin, D. J. *J. Electroanal. Chem.* **2004**, *570*, 157.

(21) Sanchez, C.; Leiva, E. P. M. *Electrochim. Acta* **1999**, *45*, 691.

(22) (a) Rooryck, V.; Reniers, F.; Buess-Herman, C.; Attard, G. A.; Yang, X. *J. Electroanal. Chem.* **2000**, *482*, 93. (b) Garcia, S.; Salinas, D.; Mayer, C.; Schmidt, E.; Staikov, G.; Lorenz, W. J. *Electrochim. Acta* **1998**, *43*, 3007.

(23) Giménez, M. C.; Del Pópolo, M. G.; Leiva, E. P. M.; García, S. G.; Salinas, D. R.; Mayer, C. E.; Lorenz, W. J. *J. Electrochem. Soc.* **2002**, *149*, E109.

(24) Grzelczak, M.; Pérez-Juste, J.; Rodríguez-González, B.; Liz-Marzán, L. M. *J. Mater. Chem.* **2006**, *16*, 3946.

(25) (a) Seo, D.; Yoo, C. I.; Jung, J.; Song, H. *J. Am. Chem. Soc.* **2008**, *130*, 2940. (b) Habas, S. E.; Lee, H.; Radmilovic, V.; Somorjai, G. A.; Yang, P. *Nat. Mater.* **2007**, *6*, 692.

(26) (a) Tsuji, M.; Miyamae, N.; Lim, S.; Kimura, K.; Zhang, X.; Hikino, S.; Nishio, M. *Cryst. Growth Des.* **2006**, *6*, 1801. (b) Kim, F.; Shon, K.; Wu, J.; Huang, J. *J. Am. Chem. Soc.* **2008**, *130*, 14442. (c) Khanal, B. P.; Zubarev, E. R. *J. Am. Chem. Soc.* **2008**, *130*, 12634.

JP8093337